Temporary electron localization and scattering in disordered single strands of DNA

Laurent Caron* and Léon Sanche
Groupe de Recherches en Sciences des Radiations, Faculté de médecine, Université de Sherbrooke, Sherbrooke, Québec, Canada J1H 5N4

(Received 8 November 2005; revised manuscript received 27 February 2006; published 8 June 2006)

We present a theoretical study of the effect of structural and base sequence disorders on the transport properties of nonthermal electron scattering within and from single strands of DNA. The calculations are based on our recently developed formalism to treat multiple elastic scattering from simplified pseudomolecular DNA subunits. Structural disorder is shown to increase both the elastic scattering cross section and the attachment probability on the bases at low energy. Sequence disorder, however, has no significant effect.

DOI: 10.1103/PhysRevA.73.062707 PACS number(s): 34.80.Bm, 87.64.Bx

I. INTRODUCTION

The electron transport properties of DNA have attracted much interest owing to the role they may play in the damage and repair of the molecule in biological cells as well as due to their potential applications in molecular electronics [1–11]. Most studies have been concerned with thermal or near thermal electron conduction. The possible mechanisms which have been proposed to explain the long-range charge transport properties in homogeneous DNA include band resonant tunneling [5,12] and polaron drifting [13] and hopping [7,14,15]. Electron trapping has been found to result essentially from intrinsic dynamic disorder due to thermal fluctuations [16].

Nonthermal electron transport within DNA is also of considerable importance to a number of applications related to photoelectron injection into the molecule [17], the formation of ballistic electrons at organic molecular interfaces [18], and radiobiological damage (for a review, see Ref. [19]). In recent investigations of strand breaks induced in DNA by 0.1 to 20 eV electrons, it has been shown experimentally that when such particles scatter within DNA, they can temporarily localize on basic subunits of the molecule (i.e., a base, the sugar ring, or the phosphate group) [20–22] and can also transfer from one subunit to another [22,23]. These studies have been followed by model calculations of electron scattering from and within DNA [24–26]. They revealed that below 15 eV an electron incident on DNA is likely to undergo multiple intersite scattering leading to constructive or destructive interferences of the wave function, depending on its energy. The new diffracted wave then interacts at a specific site, where it can be temporarily localized into a resonance state. Thus, the transport of nonthermal electrons within DNA includes diffraction along the chains and temporary capture at specific subunits.

As in the case of thermal charge carriers [16], the transport properties of 0.1 to 15 eV electrons within DNA are expected to be modified by thermal or structural disorder. In fact, from their photoinjection experiment [17], Ray *et al.* recently found temporarily electron localization to depend on the amount of disorder within DNA. They reported low-energy electron photoemission spectroscopy measurements on self-assembled monolayers (SAM) of DNA oligomers. Transient electron capture by SAM of single-stranded (ss) oligomers was found to be larger than for double-stranded (ds) ones. They conjectured that this was caused by the presumed disorder in the ss oligomers which are less rigid than the ds ones. They cited previous results [27] obtained using the same technique which showed increased scattering due to disorder in organic thin films. This is an interesting proposition, linking increased scattering to increased temporary electron capture probability. It is however uncertain if this association infallibly exists.

It is well known that disorder increases the electron elastic cross section in three-dimensional (3D) solids [28]. This has also been observed in thin films of xenon by our group [29] a number of years ago. Furthermore, disorder can lead to temporary localization of the electron's wave function in noncrystalline solids [30]. It is thus natural that such a localized state should favor electron capture. If the band is wide, localization occurs only at the band edges [30]. At energies above the vacuum level, where the bands are in the continuum, it is not expected that states would be localized in the Mott sense. But this concept of Mott localization may not apply to self-assembled films which should have some degree of organization.

What happens in the case of oligomers? Can they support localized states? Oligomers can be considered to be one-dimensional (1D) molecular constructions. The overlapping molecular states form 1D bands. It is known that disorder usually totally localizes the electron bands in 1D systems [31]. Even for a short oligomer one might still get localized Mott-like states for a strong enough variation of the molecular species along its length. At energies above vacuum, shape resonances can also acquire a band character [32]. Motion of electron-exciton complexes formed from overlapping core excited resonances [33] has been observed in rare gas [34,35] and organic films [36,37]. For electron energies above the vacuum level, the oligomer band states are immersed in the continuum. Shape resonances have a finite lifetime and can only lead to bands if the electron transfer time between molecular wave functions is much shorter than the lifetime. This is normally the case. So localization within oligomers or

*Permanent address: Département de physique et Regroupement québécois sur les matériaux de pointe, Université de Sherbrooke, Sherbrooke, Québec, Canada J1K 2R1. Electronic address: caron@physique.usherbrooke.ca

polymers above vacuum is probably controlled more by molecular disorder than by lifetime. A stronger disorder implies a more localized state and should favor capture. But this is the back end of the capture process. At the front end of the process, a continuum electron scatters on the oligomer and eventual transfers onto a metastable quasibound localized oligomer state. This process involves the electron wave function amplitude at the molecular subunits of the oligomer as a preamble to the transfer. This entrance wave function is also affected by any disorder in the oligomer. In this paper, we wish to study this front end aspect of electron capture for a single strand of the DNA molecule.

For this purpose, we use the formalism we have developed for our previous studies of elastic scattering on DNA [24–26]. It allows us to deduce general trends related to the structural aspects of helical macromolecules, disorder being one of these. In the next section, we review the basic aspects of our model. We then present its implementation to a simplified model of the type of ss oligomers investigated by Ray *et al.* [17]. We next present the results of the simulation runs for structural and base sequence disorders. A conclusion is added at the end.

II. MODEL

A. Multiple scattering theory

In Refs. [24,25], we presented the basic equations for multiple electron scattering within macromolecules, including DNA. For the latter, we proposed a simple model of molecular subunits (i.e., bases, sugars, and phosphates) immersed in an optical potential U_{op}, which is constant between their R-matrix shells (or between the muffin tins), a working hypothesis that has been used in the calculations for simple molecules [38] and in the theory of low-energy electron diffraction in solids [39]. One can quite generally describe the scattering problem of a molecular subunit by its scattering matrix $S_{LL'}$ [40,41] where $L=(l,m)$ are the angular momentum quantum numbers. Each molecular subunit has an incident plane wave of momentum $\vec{k}$ impinging on it plus the scattered waves of all other subunits. More specifically, we described the asymptotic form of the total wave function $\psi_{\vec{k}}^{(n)}(\vec{r})$ for a molecule centered at $\vec{R}_n$ outside the R-matrix shell by the following equation:

$$\psi_{\vec{k}}^{(n)}(\vec{r}) = 4\pi e^{i\vec{k}\cdot\vec{R}_n}\sum_{LL'} i^l B_{\vec{k}L}^{(n)} Y_{L'}(\Omega_{\vec{r}_n}) \times\left[j_l(kr_n)\delta_{LL'} + \tfrac{1}{2}(S_{LL'}^{(n)} - \delta_{LL'})h_{l'}^{+}(kr_n)\right], \quad (1)$$

where Y_L are spherical harmonics, j_l and $h_{l'}^{+}$ are the spherical Bessel function and Hankel function of the first kind respectively, $\vec{r}_n=\vec{r}-\vec{R}_n$, and

$$B_{\vec{k}L}^{(n)} = Y_L^*(\Omega_{\vec{k}}) + \frac{1}{2}\sum_{n'\neq n}\sum_{L_1,L_2,L_2'} i^{l_1+l_2-l_2'} B_{\vec{k}L_2}^{(n')}(S_{L_2L_2'}^{(n')} - \delta_{L_2L_2'}) \times(-1)^{m_2'} e^{-i\vec{k}\cdot\vec{R}_{nn'}} F_{m_1,m,-m_2'}^{l_1,l,l_2'} Y_{L_1}(\Omega_{\vec{R}_{nn'}}) h_{l_1}^{+}(kR_{nn'}), \quad (2)$$

where

$$F_{m_1,m_2,m_3}^{l_1,l_2,l_3} = [4\pi(2l_1+1)(2l_2+1)(2l_3+1)]^{1/2} \times\begin{pmatrix} l_1 & l_2 & l_3 \\ 0 & 0 & 0 \end{pmatrix}\begin{pmatrix} l_1 & l_2 & l_3 \\ m_1 & m_2 & m_3 \end{pmatrix},$$

and $\begin{pmatrix} l_1 & l_2 & l_3 \\ m_1 & m_2 & m_3 \end{pmatrix}$ is the Wigner 3-j symbol [42], and $\vec{R}_{nn'}=\vec{R}_n-\vec{R}_{n'}$. Equation (2) implies a coupled set of linear equations for all $B_{\vec{k}L}^{(n)}$. As mentioned before [24,25], this would prove arduous if not impossible to solve for large macromolecules were it not for the loss of coherence of the electrons due to inelastic collisions and to the presence of parasite scatterers (e.g., the water molecules in the grooves could be considered as such). These processes can be invoked through an imaginary part in the background optical potential U_{op} [39], i.e., an imaginary part to the electron wave number $\mathrm{Im}(k)=\xi^{-1}$. Here ξ acts as a coherence length for the electrons. This representation allows approximate, though accurate, *local* solutions by truncated finite-size matrices containing the information for the number of subunits within a few coherence lengths. For finite-size molecules, as is the case here, there is no computational need for a finite coherence length. So we shall ignore it, i.e., set it to infinity.

B. Electron capture and scattering

In an effort to extract physically meaningful information from the multiple scattering formalism, we had previously targeted a calculation of the capture amplitude $V_{\vec{k}}^{(c)}$ of an electron in a shape or core excited resonance of a basic subunit C positioned at $\vec{R}_c$. We had assumed a dominant capture channel symmetry corresponding to L_o and had used the one center approximation of O'Malley [43]. When generalized to a multiple scattering situation, this led to

$$V_{\vec{k}}^{(c)} = \sqrt{4\pi}V_{L_o}(C_{\vec{k}L_o} + Y_{L_o}^*(\Omega_{\vec{k}}))e^{i\vec{k}\cdot\vec{R}_c}, \quad (3)$$

where

$$C_{\vec{k}L} = \frac{1}{2}\sum_{n'\neq C}\sum_{L_1,L_2,L_2'} i^{l_1+l_2-l_2'} B_{\vec{k}L_2}^{(n')}(S_{L_2L_2'}^{(n')} - \delta_{L_2L_2'}) \times(-1)^{m_2'} e^{-i\vec{k}\cdot\vec{R}_{Cn'}} F_{m_1,m,-m_2'}^{l_1,l,l_2'} Y_{L_1}(\Omega_{\vec{R}_{Cn'}}) h_{l_1}^{+}(kR_{Cn'}), \quad (4)$$

and V_{L_o} is an energy and nuclear coordinate dependent amplitude. There is unfortunately no available theoretical information on the nuclear part for the DNA bases at this time although calculations are forthcoming [44,45]. So we shall only focus on the electronic part. These equations are obtained by expanding the electronic wave function around $\vec{R}_c$.

We proposed [26] a weighted partial capture factor

$$\Gamma_w(l_o) = \frac{\sum_{\vec{R}_C}\gamma(l_o,\vec{R}_C)}{\sum_{\vec{R}_C}}, \quad (5)$$

with

$$\gamma(l_o,\vec{R}_C)=\frac{\sum_{m_o}|\sqrt{4\pi}(C_{\vec{k}l_om_o}+Y^*_{l_om_o}(\Omega_{\vec{k}}))e^{i\vec{k}\cdot\vec{R}_C}|^2}{\sum_{m_o}|\sqrt{4\pi}Y^*_{l_om_o}(\Omega_{\vec{k}})e^{i\vec{k}\cdot\vec{R}_C}|^2}, \quad (6)$$

which measures the partial wave decomposition of the total wave function averaged over the different chosen positions $\vec{R}_C$. Here the sum over $\vec{R}_C$ runs over all selected subunits while the sum over m_o runs from $-l_o$ to l_o. The weighting factor in Eq. (6) (the denominator) has the extra property that it is independent of $\hat{k}$. This would serve as meaningful measures of the effect of multiple scattering on the capture probability in the l_o channel for both types of resonances. Note that $\Gamma_w(0)$ equals the average absolute square of the wave function.

We also propose to calculate, for a finite size molecule, the scattering cross section σ_e. The total scattered wave function is obtained by summing the second term on the right hand side of (1) (the one with $h^+_{l'}$) over all scatterers.

III. SIMULATION

The present formulation is specialized to decamers (10 PBS), short oligomers of the type used in Ref. [17], mimicking the structure of a segment of single strand DNA. It is made of pseudobases (PBS) chemically bonded to a common pseudobackbone (PB). These PBS and backbone are constructed, as before, from centrosymmetric scatterers. The PBS are the same as in Refs. [24,25] and consists of coplanar PC and PG arrangements of scatterers resembling the cytosine and guanine (C and G) base units of DNA [46]. Their arrangement relative to the backbone is, however, different having to link to a common backbone whose structure we wish to keep independent of the PBS used. This is shown in Fig. 1. The PB [26] is composed of 11 scatterers which are ordered to simulate the spatial arrangement of the sugar-phosphate units [46] and the average inter-PBS distance of DNA. The sum over n in Eqs. (2) or (4) and in Eq. (1), for the calculation of σ_e, then runs over the individual scatterers. Moreover, for single centrosymmetric scatterers, one has $\frac{1}{2}(S^{(n')}_{LL'}-\delta_{LL'})=i\delta_{LL'}e^{i\delta_{nl}}\sin(\delta_{nl})$ where δ_{nl} is the nth scatterer phase shift. We have used the phase shifts of Ar [47] for all scatterers as in our previous calculations.

The parameters of ss DNA were the following: a screw pitch of $c=3.4$ nm and a number of bases per turn $N_c=10$ which are characteristic of the B form of DNA, the $l=0,1,2$ phase shifts of the electronically inert species Argon. As the decamers are very short, we have already mentioned that we have used $\xi=\infty$.

In order to study the effect of structural disorder in ss DNA, we have considered two types of changes from regular helical positions. The first one is orientation disorder. It preserves the coplanar shape of the PBS and leaves the anchor position to the PB fixed (see Fig. 1). It consists of a tilt, which lifts the end of the PBS principal axis in the helical axis direction, a twist, which moves it in its plane, and a roll, which rotates the PBS. We have chosen a uniform random distribution in the interval ±20° for twist and roll and ±10° for tilt for the 10 PBS making up the decamer. The second type of disorder originates in the backbone which, at each segment of the decamer, is rotated around the axis connecting two successive sugar 3′-O atoms and moves its PBS along with it. This PB segment motion is accompanied by azimuthal and polar displacements. This results in a global tilt, twist, and roll of the PBS plus backbone disorder. We have chosen a uniform random distribution in the intervals ±20° for rotation and azimuthal change and a linearly increasing 0°–10° change from bottom to top of the decamer for the polar angle. This morphology reproduces the type of "mushroom" disorder and resulting reduction in vertical size observed by Ray *et al.* [48] in their oligomer films. Figure 2 shows a side perspective of the three decamers described here.

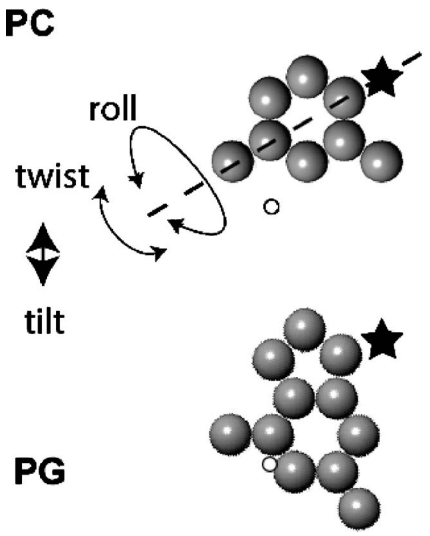

FIG. 1. Structural arrangement of the scatterers in the PC and PG pseudobases and their relative positioning with respect to the anchor position on the backbone (star). The open circle lies at the position of the axis of the helix. The three basic motions of the PC relative to its anchor are illustrated. The dashed line is the axis which defines these movements.

In our past work, we had chosen the incident direction to be perpendicular to the axis of helix. This time we choose the incident electrons to be along the axis of the decamer as in the photoelectron injection experiments of Ray *et al.* [17].

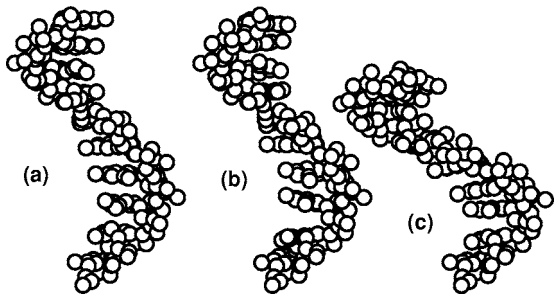

FIG. 2. Side perspective of the three different all PC decamers used: (a) regular helical placement, (b) helical PB with PC orientation disorder, and (c) PB disorder resulting in the "mushroom" arrangement.

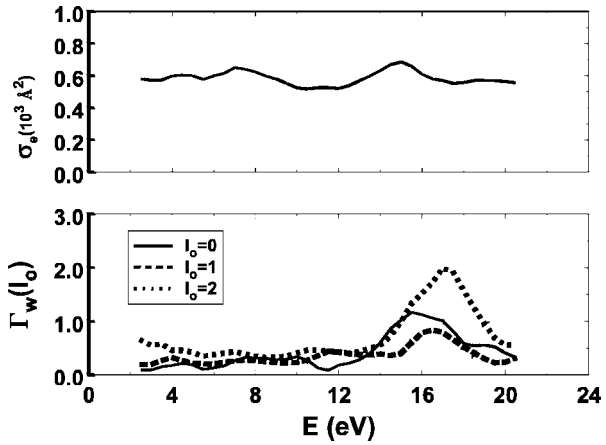

FIG. 3. Elastic cross section and weighted partial capture factors for a single helically ordered ss decamer with all PC pseudobases as a function of energy.

IV. RESULTS AND DISCUSSION

Figure 3 shows the elastic cross section and weighted partial capture factor (partial wave decomposition) at the center of the hexagonal ring for the regular all PC decamer of Fig. 2(a). There is only weak modulation at low energy. A broad peak is seen in $\Gamma_w(l_o)$ between 14 and 20 eV which is due to the combined influence of the PB and PBS (see discussion later). A hump is seen in the cross section at 15 eV. This is characteristic of the backbone whose elastic cross section, shown in Fig. 4, also has a hump at that energy. One notes that the lower energy hump of the backbone is not seen in Fig. 3. *There appears to be some destructive interference between the PBS and PB at low energies*. Curiously, there is no clear sign of the internal diffraction peak which was observable in the 12–15 eV range for perpendicular incidence [25,26]. It is most clearly visible along the axis direction, at $\theta=0°$. It can be seen in Fig. 5 as a narrow peak at 15 eV in the differential cross section $(d\sigma_e/d\Omega)_{\theta=0}$. It could well be hidden within the hump in σ_e at 15 eV.

Figure 6 shows the effect of the orientation disorder corresponding to the all PC decamer of Fig. 2(b). There is a substantial overall increase in σ_e while $\Gamma_w(l_o)$ shows a remarkable increase below 10 eV and a decrease in the higher energy peak. *This disorder restores the lower energy contribution to σ_e of the PB of Fig. 4 by presumably neutralizing the interference with the PB in the regular PBS array*. The effect of the PB disorder of Fig. 2(c) on σ_e and $\Gamma_w(l_o)$, in Fig. 7, is similar. The contribution of the disordered PB to the elastic cross section is featureless, however, as seen in Fig. 4. Therefore, the details in the σ_e curve of Fig. 7 originate from the PBS which show low-energy humps similar to those of Fig. 6, though of reduced amplitude (note the reduced vertical scale). The zigzag pattern seen in $\Gamma_w(0)$ of Fig. 7 at around 4 eV can even be observed in σ_e of the same figure. One must remember there is dominant s-wave scattering at low energy. The higher angular momentum components play a secondary role in the elastic cross section at low energy. But they are of primary importance in attachment processes to low-energy shape resonances. Note that the height of the internal diffraction peak which appears at 15 eV in Fig. 5,

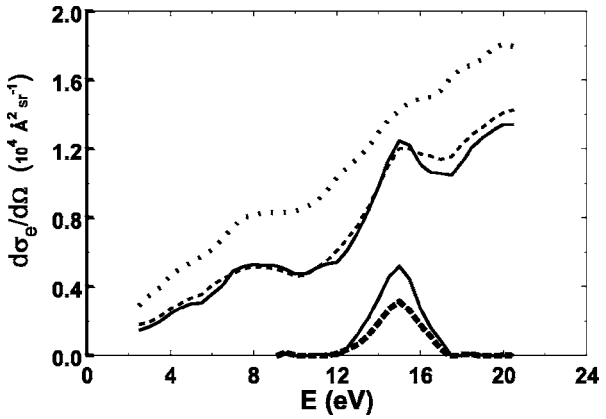

FIG. 5. Differential cross section for elastic scattering in the forward direction from a single helically ordered (full line), orientation disordered (dashed line), and pseudobackbone disordered (dotted line) ss decamer with all PC pseudobases as a function of energy. The bell shaped curves on the bottom part show the diffraction peaks stripped of the background.

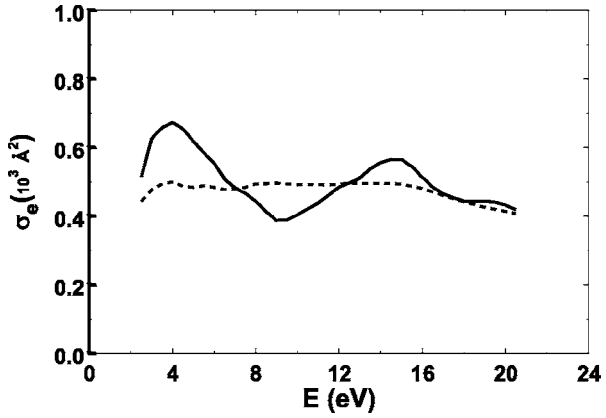

FIG. 4. Elastic cross section for the helical pseudobackbone (solid line) and the disordered one (dashed line) as a function of energy.

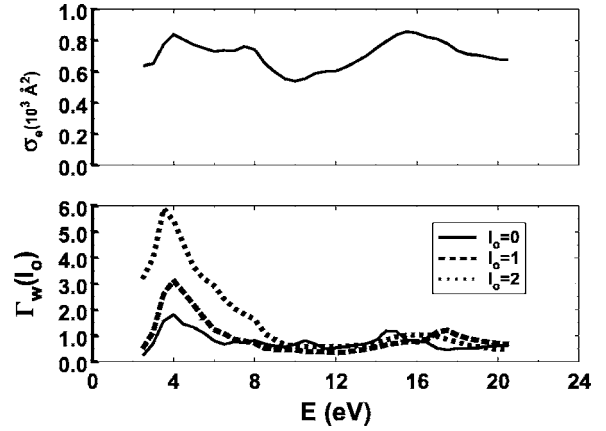

FIG. 6. Elastic cross section and weighted partial capture factors for a single ss decamer with orientation disordered PC pseudobases as a function of energy.

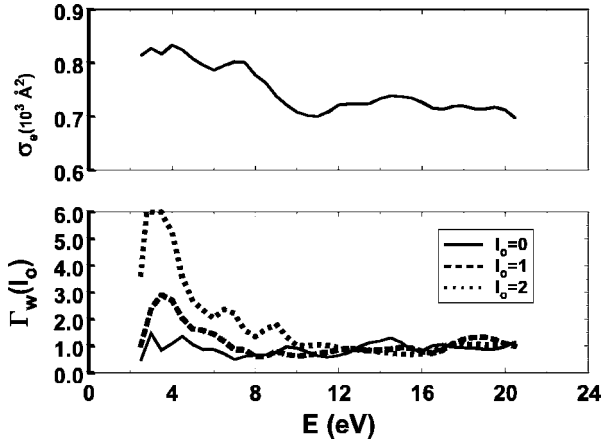

FIG. 7. Elastic cross section and weighted partial capture factors for a single ss decamer with disordered pseudobackbone and all PC pseudobases as a function of energy. Note the reduced range in the scale of the cross section.

has its amplitude reduced by almost a factor of 2 for orientation disorder and is difficult to evaluate for PB disorder.

The low-energy peaks in $\Gamma_w(l_o)$ for $l_o=1,2$ warrant a closer look. One might wonder if there is not some destructive interference in the well ordered configuration which quenches them. We do not believe this to be the case. First, $\Gamma_w(l_o)$ is quite uneventful over a broad range below 10 eV in Fig. 3. There is no sign of anything particularly "destructive" occurring around 4 eV, at twice the wavelength of the internal diffraction peak. Second, we have evidence that the low-energy peaks are related to the regions, in the disordered PBS, in which the pseudobases are more closely spaced. This evidence comes from the separate study of the decamers without the PB. Figure 8 shows the $\Gamma_w(l_o)$ with only the pseudobases present. The high-energy peak is quite subdued showing that the PB plays a large role in its definition. The low-energy peaks behave in quite a similar fashion as with the PB in Figs. 3, 6, and 7. They are thus clearly coming

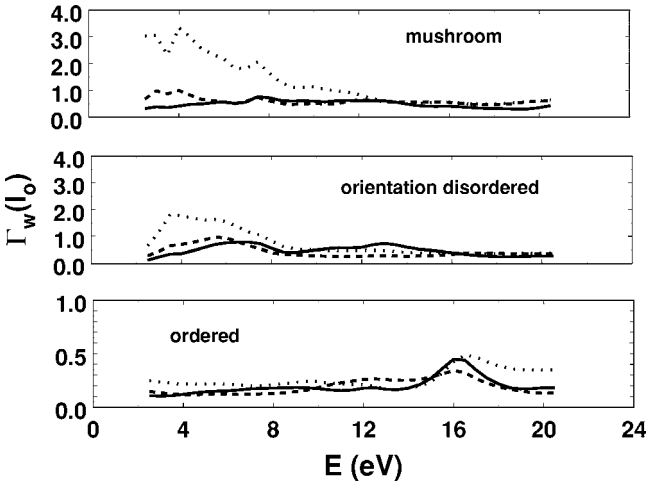

FIG. 8. Weighted partial capture factors for three arrays of PC pseudobases only (without the pseudobackbone) as a function of energy for three values of $l_o=0$ (full line), 1 (dashed line), and 2 (dotted line).

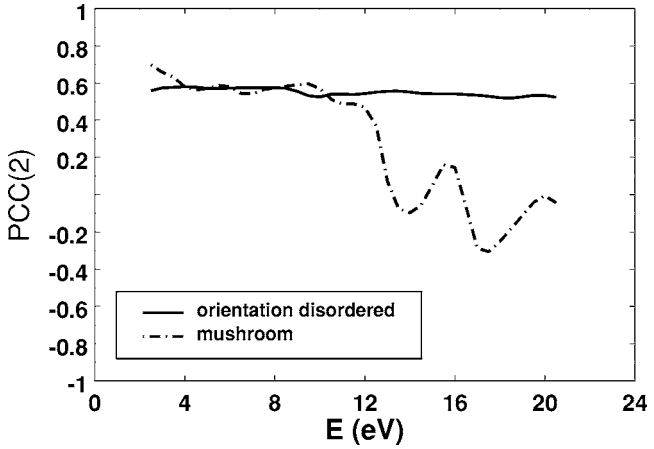

FIG. 9. Pearson correlation coefficient of nearest-neighbor weighted partial capture factor product with decrease of interring distance for $l_o=2$.

from the PBS. We can correlate them with the more closely spaced PBS. In order to show this, let us define the Pearson correlation coefficient *PCC* between the neighboring bases pair product $\gamma(l_o,n)\gamma(l_o,n+1)$ and their relative distance contraction $(\bar{d}-d_{n,n+1})$

$$PCC(l_o) = \frac{\sum_{n=1}^{9}(\gamma(l_o,n)\gamma(l_o,n+1)-\overline{\gamma\gamma})(\bar{d}-d_{n,n+1})}{\sqrt{\sum_{n=1}^{9}(\gamma(l_o,n)\gamma(l_o,n+1)-\overline{\gamma\gamma})^2}\sqrt{\sum_{n=1}^{9}(\bar{d}-d_{n,n+1})^2}},$$

where $\gamma(l_o,n)$ is defined in Eq. (6), with $\vec{R}_C$ here represented by the index n of the PB, $\overline{\gamma\gamma}$ is the average of the pair products, $d_{n,n+1}$ is the distance between neighboring ring centers, and $\bar{d}$ is its average. This coefficient provides a measure of the correlation between the peaks and the PBS pair distance. A value of one implies total correlation while a value of zero means the two variables are uncorrelated. Figure 9 shows the correlation coefficients for the disordered situations and for $l_o=2$. Very similar results are obtained for the other values of angular momentum. There is good correlation at low energy which indicates that *the peaks are caused by local clumping of the PBS in the disordered decamers*. These can be seen in Fig. 2. They very likely correspond to inter-PB resonances corresponding to the high energy tail of Mott localized states, mentioned at the end of the Introduction, which would result from such "clumping."

In order to check on the effect of collective interoligomer interference, we have looked at three regular decamers arranged in a triangular array with 45 atomic units (a.u.), i.e., Bohr radii distance one from another. This would correspond to what an electron would see of the film within a coherence length less than 80 a.u. The elastic cross section is roughly three times that of a single decamer and the partial capture factors are nearly the same. There is no clear sign of interdecamer interference. We have repeated this for three decam-

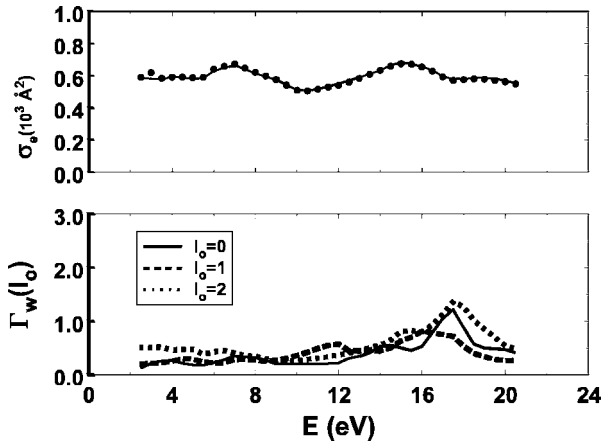

FIG. 10. Elastic cross section and weighted partial capture factors for a single regular helical decamer of pseudo-DNA with a random sequence of equal numbers of PC and PG pseudobases as a function of energy. The dots in the upper figure represent the average elastic cross section of all PC and all PG decamers.

ers with backbone disorder at the same distance one from the other and rotated around the vertical axis by 40°. The same observations prevail.

It thus seems quite general that disorder leads to an increased scattering and an increased partial capture factor at low energy. This suspected but unproven association between the two physical quantities mentioned in the Introduction is thus verified.

We have finally done calculations for a decamer with sequence disorder. Equal numbers of PC and PG PBS were randomly mixed. The results are shown in Fig. 10. The elastic cross section is, oddly enough, incredibly close to the average value for all PC and all PG decamers. The partial capture factor is also similar, though not exactly equal, to the average one. Sequence disorder thus does not produce significant variations beyond averaging for regularly positioned PBS.

V. CONCLUSION

In our previous theoretical studies [24–26], we have investigated the interaction of nonthermal electrons with models of the DNA bases with and without inclusion of the backbone. The DNA was taken to be in the double stranded configuration and disorder was not systematically introduced in our models. In the present investigation, we introduced into a single strand of DNA sequence and topological disorder. The latter consist of a random distribution of twist, roll, and tilt motion of the bases and the backbone. Since in the double stranded configuration DNA is much more rigid, and thus less prone to disorder, we chose a decamer of single stranded DNA for this type of calculations.

The elastic cross section and capture factors are affected by disorder due to a combination of two effects: loss of long-range coherence and enhanced short-range scattering. The overall picture is that structural disorder tends to destroy the long-range interference between and within the bases and backbone, most noticeably reducing the internal diffraction at the higher energies, while the short-range disorder globally increases the elastic scattering cross section and produces local low-energy resonances. This increase in both the elastic scattering cross section and the capture amplitude at the lower energies supports the hypothesis of Ray *et al.* [17], linking disorder to increased capture amplitude. Lastly, pure sequence disorder does not lead to a significant enhancement of elastic scattering and interference in the partial wave functions and there is no clear evidence of interdecamer interference patterns.

It should be noted that in single stranded DNA, thermal motion not only produces disorder in the pattern of DNA constituents, but populates vibrational levels of these constituents lying at energies above that of the ground vibrational state. Such a temperature effect is well known from gas-phase experiments with small molecules [49]. Basically, increasing the temperature increases the Franck-Condon (F-C) width for the transition from the ground state of the molecule to the transient anion state. Usually, the larger F-C width causes an increase in the electron capture cross section and a modification of the branching ratios for all decay channels. The effect is particularly pronounced in the DEA channel, if the increase in F-C width, for a transition to a dissociating anion state, causes the transition to occur at internuclear distances close to those required for stabilization of the extra electron on one of the fragments. In this case, a strong enhancement in the DEA cross section occurs [49]. Thus, in a more elaborate treatment of temperature effects on DNA damage, the influence of the vibrational population of the basic constituents on the cross sections for electron capture and bond scission should be taken into account. This is necessary for a more adequate comparison between theoretical calculations and experiments performed at room temperature on LEE-induced DNA damage [1,19].

ACKNOWLEDGMENTS

We wish to thank Dr. R. Naaman for providing the information on the shape of the oligomers in the photoelectron injection experiments. This research was financed by the Canadian Institute of Health Research.

[1] L. Sanche, Mass Spectrom. Rev. **21**, 349 (2002).
[2] C. Dekker and M. A. Ratner, Phys. World **8**, 29 (2001).
[3] P. J. de Pablo, F. Moreno-Herrero, J. Colchero, J. G. Herrero, P. Herrero, A. M. Bar, P. Ordejón, J. M. Soler, and E. Artacho, Phys. Rev. Lett. **85**, 4992 (2000).
[4] A. J. Storm, J. van Noort, S. de Vries, and C. Dekker, Appl. Phys. Lett. **79**, 3881 (2001).
[5] D. Porath, A. Bezryadin, S. de Vries, and C. Dekker, Nature

(London) **403**, 635 (2000).
[6] L. Cai, H. Tabata, and T. Kawai, Appl. Phys. Lett. **77**, 3105 (2000).
[7] K.-H. Yoo, D. H. Ha, J.-O. Lee, J. W. Park, J. Kim, J. J. Kim, H.-Y. Lee, T. Kawai, and H. Y. Choi, Phys. Rev. Lett. **87**, 198102 (2001).
[8] H.-W. Fink and C. Schönenberger, Nature (London) **398**, 407 (1999).
[9] Y. Okahata, T. Kobayashi, K. Tanaka, and M. Shimomura, J. Am. Chem. Soc. **120**, 6165 (1998).
[10] A. Y. Kasumov, M. Kociak, S. Gueron, B. Reulet, V. T. Volkov, D. V. Klinov, and H. Bouchiat, Science **291**, 280 (2001).
[11] H. Tabata, L. T. Cai, J. H. Gu, S. Tanaka, Y. Otsuka, Y. Sacho, M. Taniguchi, and T. Kawai, Synth. Met. **133-134**, 469 (2003).
[12] M. Hjort and S. Stafström, Phys. Rev. Lett. **87**, 228101 (2001).
[13] S. V. Rakhmanova and E. M. Conwell, J. Phys. Chem. B **105**, 2056 (2001).
[14] G. B. Schuster, Acc. Chem. Res. **33**, 253 (2000).
[15] P. T. Henderson, D. Jones, G. Hampikian, Y. Kan, and G. B. Schuster, Proc. Natl. Acad. Sci. U.S.A. **96**, 8353 (1999).
[16] G. Kalosakas, K. O. Rasmussen, and A. Bishop, Acc. Chem. Res. **33**, 253 (2003).
[17] S. Ray, S. Daube, and R. Naaman, Proc. Natl. Acad. Sci. U.S.A. **102**, 15 (2005).
[18] H. E. Katz, A. J. Lovinger, J. Johnson, C. Kloc, T. Siegrist, W. Li, Y.-Y. Lin, and A. Dodabalapur, Nature (London) **404**, 478 (2000).
[19] L. Sanche, Eur. Phys. J. D **35**, 367 (2005).
[20] B. Boudaïffa, P. Cloutier, D. Hunting, M. A. Huels, and L. Sanche, Science **287**, 1658 (2000).
[21] X. Pan, P. Cloutier, D. Hunting, and L. Sanche, Phys. Rev. Lett. **90**, 208102 (2003).
[22] F. Martin, P. D. Burrow, Z. Cai, P. Cloutier, D. Hunting, and L. Sanche, Phys. Rev. Lett. **93**, 068101 (2004).
[23] Y. Zheng, P. Cloutier, D. Hunting, R. Wagner, and L. Sanche, J. Am. Chem. Soc. **127**, 16592 (2005).
[24] L. G. Caron and L. Sanche, Phys. Rev. Lett. **91**, 113201 (2003).
[25] L. Caron and L. Sanche, Phys. Rev. A **70**, 032719 (2004).
[26] L. Caron and L. Sanche, Phys. Rev. A **72**, 032726 (2005).
[27] R. Naaman and Z. Vager, Acc. Chem. Res. **36**, 291 (2003).
[28] R. A. Smith, *Wave Mechanics of Crystalline Solids* (Chapman and Hall, London, 1961).
[29] G. Bader, G. Perluzzo, L. G. Caron, and L. Sanche, Phys. Rev. B **26**, 6019 (1982).
[30] N. F. Mott and E. A. Davis, *Electronic Processes in Noncrystalline Materials* (Clarendon Press, Oxford, 1979), 2nd edition.
[31] N. F. Mott and W. D. Twose, Adv. Phys. **10**, 107 (1961).
[32] L. G. Caron, G. Perluzzo, G. Bader, and L. Sanche, Phys. Rev. B **33**, 3027 (1986).
[33] G. Bader and L. G. Caron, J. Chem. Phys. **77**, 3166 (1982).
[34] P. Rowntree, H. Sambe, L. Parenteau, and L. Sanche, Phys. Rev. B **47**, 4537 (1993).
[35] M. A. Huels, P. Rowntree, L. Parenteau, and L. Sanche, Surf. Sci. **390**, 282 (1997).
[36] G. Bader, L. G. Caron, and L. Sanche, Solid State Commun. **38**, 849 (1981).
[37] L. G. Caron and G. Bader, J. Chem. Phys. **80**, 119 (1984).
[38] D. Dill and J. L. Dehmer, J. Chem. Phys. **61**, 692 (1974).
[39] J. B. Pendry, *Low Energy Electron Diffraction* (Academic, London, 1974).
[40] N. F. Mott and H. S. W. Massey, *The Theory of Atomic Collisions* (Clarendon, Oxford, 1965), 3rd edition.
[41] F. A. Gianturco and A. Jain, Phys. Rep. **143**, 347 (1986).
[42] A. Messiah, *Quantum Mechanics* (Wiley, New York, 1962), Appendix C.
[43] T. F. O'Malley and H. S. Taylor, Phys. Rev. **176**, 207 (1968).
[44] C. Tonzani and C. H. Greene, J. Chem. Phys. **126**, 054312 (2006).
[45] V. McKoy and C. Winstead, *Electron Collisions with Large Molecules: Computational Advances*, Technical Program: 231st National Meeting of the American Chemical Society, Atlanta, GA (2006).
[46] R. L. P. Adams, J. T. Knowler, and D. P. Leader, *The Biochemistry of the Nucleic Acids* (Chapman and Hall, New York, 1981), Tenth edition.
[47] M. Michaud, L. Sanche, C. Gaubert, and R. Baudoing, Surf. Sci. **205**, 447 (1988).
[48] S. G. Ray, S. S. Daube, G. Leitus, Z. Vager, and R. Naaman, Phys. Rev. Lett. **96**, 036101 (2006).
[49] H. Hotop, M.-W. Ruf, M. Allan, and I. I. Fabrikant, Adv. At., Mol., Opt. Phys. **49**, 85 (2003).